Severe Damage of a Pile Group due to Slope Failure

Author

Ong, DEL, Leung, CF, Chow, YK, Ng, TG

Published

2015

Journal Title

Journal of Geotechnical and Geoenvironmental Engineering

Version

Accepted Manuscript (AM)

DOI

10.1061/(ASCE)GT.1943-5606.0001294

Severe Damage of a Pile Group Due to Slope Failure

D E L Ong[1]; C F Leung[2], Y K Chow[3] and T G Ng[4]

Abstract: A pile group consisting of four cast in-place concrete piles was instrumented to measure the induced bending moment along the piles due to excavation of an adjacent slope. The green field lateral soil movement profiles and the lateral pile deflection profiles were monitored by in-soil and in-pile inclinometers, respectively. The unexpected early arrival of rain storm prior to the year-end monsoon caused the failure of the slope which resulted in the severe damage of this pile group located at the slope crest. This paper examines the pre- and post-failure behavior of the pile group and it is demonstrated that considering the uncracked and cracked bending stiffness of the piles is vital when evaluating the progressive damage of the pile group due to slope failure.

Keywords: Bending moment; Pile Group; Deflection; Excavation; Lateral soil movement, Limiting soil stress, Back-analysis; Pile cracks

[1]Director (Acting), Research Centre for Sustainable Technologies, Faculty of Engineering, Science & Computing, Swinburne University of Technology, Sarawak Campus, 93350 Kuching, Sarawak, Malaysia. E-mail: elong@swinburne.edu.my

[2]Professor, Centre for Soft Ground Engineering, Civil Engineering Dept., National University of Singapore, Singapore 117576. E-mail: ceelcf@nus.edu.sg

[3]Professor, Centre for Soft Ground Engineering, Civil Engineering Dept., National University of Singapore, Singapore 117576. E-mail: ceechow@nus.edu.sg

[4]Executive Director, GeoEng Consultants (S) Pte Ltd./ Golder Associates (S) Pte Ltd., Singapore 329983. E-mail: ngtg@golder.com.sg

Introduction

A proposed 8-storey industrial building with a one-level basement car park was constructed on an approximately 15,000 m^2 site in Singapore. An instrumented cast in-place concrete pile group comprising four 900-mm diameter piles was constructed near to the proposed access road boundary. In order to facilitate the construction of an underground storage tank, excavation in front of the instrumented pile group with slope gradient of 1:2.5 (vertical:horizontal) was carried out in marine clay. The maximum excavation depth was about 6 m below the existing ground level. Due to the unexpected early arrival of rain storm prior to the year-end monsoon season, the slope failed and the resulting excessive soil movement led to failure of the instrumented pile group.

The failure of the instrumented pile group was characterized by relatively large pile deflections as a direct result of lateral soil movements due to the slope failure. The field data obtained was evaluated in detail to achieve a better understanding on the magnitude of limiting soil stress on a pile group to reinforce the findings from centrifuge model studies on excavation-induced soil movement on a single pile (Ong et al. 2006; Leung et al. 2006) and on pile groups (Ong et al. 2009, 2011). A numerical study was also conducted to back-analyze the field data to gain a deeper understanding of the complex soil-structure interaction behavior. It should be noted that the main focus of this paper is on the pile-group behavior when affected by lateral soil movements and not on the cause of the slope failure.

Soil profile

Standard penetration tests (SPT) and limited numbers of in-situ vane shear tests were carried out to investigate the underlying soft marine clay. Fig. 1 shows the plan view of the site with locations of Borehole BH1, installed instruments and the

instrumented pile group at the site. The groundwater level was measured using a standpipe piezometer installed to a depth of 25m and found to be 1 m below ground level prior to the commencement of excavation.

Fig. 2 shows the interpreted subsurface soil profile and the geotechnical properties. Underlying the 1 m thick fill layer was a 9 m thick very soft greenish grey marine clay of the Kallang Formation with standard penetration resistance (N value) less than 4. The underlying Old Alluvium was 2.5 m thick and comprised loose clayey sand with N values of 5 and 14, followed by a 1 m thick medium dense sand with N values of 14 and 38. Subsequently, a 9.5 m thick dense clayey sand with N values ranging between 29 and 50 was found. BH1 was terminated in very dense clayey sand where SPT refusals were recorded.

Instrumentation program and layout

In view of anticipated excavation in front of the piles, a pile group consisting of four 900-mm cast in-situ concrete bored piles was instrumented to measure the expected bending moment along the pile induced during and after the excavation. One front pile (nearer to the excavation) and one rear pile (further away from the excavation) were instrumented. Fig. 3 shows the plan and elevation views of the instrumented piles in relation to the excavation. The locations of the in-pile inclinometer and the strain gages are shown in Fig. 4. As it was expected that the pile segment within the marine clay layer would bend more than other segments, the elevations of the resistance-type strain gages along the two instrumented piles were planned accordingly. To ensure that the strain gages function well under harsh and damp conditions, they were carefully water-proofed using resin. The wires connecting the strain gages were properly buried underground before connecting to the strain meter which was programmed to automatically acquire the strain gage readings every

6 hours. An in-pile inclinometer was also installed in a rear pile to measure its pile deflection profile. The conventional inclinometer casing was placed in the bored pile before concreting. After concreting, baseline readings were taken. The measured pile deflection profile could then be differentiated to derive the pile bending moment profile.

Excavation sequence and construction events

Fig. 5 shows schematically the key events over the 2-month excavation and construction period. Due to the unexpected early arrival of rain storm prior to the year-end monsoon season, the slope slipped overnight after excavation of only 3.5 m from the original ground level. Fig. 6 shows the slope failure at the location of instrumented pile group. Henceforth, Day 0 is denoted as the day that slope failure occurred. It should be noted that sheet piles and steel struts were installed at the toe of the slope to protect the nearby piles only when the soil movements became unexpectedly large, especially after the occurrence of the soil slip.

Measured in-pile and in-soil inclinometer readings

The in-pile inclinometer was installed in one of the rear piles prior to the occurrence of soil slip. The measured rear pile deflection profiles are presented in Fig. 7(a). However, the in-soil inclinometer was installed 5 days after the first soil slip and the lateral soil movement profiles using Day 5 readings as datum are shown in Fig. 7(b). At the end of the monitoring period, the maximum pile deflection and the maximum lateral soil movement measured at the ground level were about 220 mm and 590 mm, respectively.

It is noted that both the pile and soil movement profiles are generally triangular in shape where the largest magnitudes are recorded at the ground level. The figures also reveal that the magnitudes of pile deflection and lateral soil movements

reduce with increasing depth until about 13 m depth. Below this depth, the magnitudes of lateral pile and soil movements quickly diminish due to stiffer resistance offered by the medium dense sand (N value of 14) to dense clayey sand (N value of 38).

Fig. 8 shows a comparison between the measured lateral pile deflection and the lateral soil movement at various depths over the excavation period. Since both the in-pile and in-soil inclinometers were located at about the same distance from the excavation, the in-soil inclinometer readings could be reasonably assumed as the green field lateral soil movements. Green field soil movements are the natural behavior of soil movement patterns in the absence of a pile. Prior to Day 14, the differences in lateral pile deflections and soil movements seemed insignificant.

However, after Day 14, it was evident that the lateral soil movement exceeded the pile deflection within the top 10 m soft marine clay layer. The difference between soil movement and pile deflection became more significant as excavation progresses. At this stage, large-strain shear deformations were experienced by the soft clay as the propped sheet pile wall failed in mitigating the lateral soil movements triggered by the soil slip and also active lateral soil stress had been fully mobilized. Therefore, increasingly more soils became plastic and subsequently flowed past the piles as evidenced by the increasingly larger lateral soil movements especially after the excavation had reached at least 5 m, as shown in Fig. 8.

Ultimate and cracking moment capacities of pile

As concrete is weak against tension, the concrete in the bored piles is expected to crack when subject to large bending strain. As the bending rigidity (EI) of cracked concrete would be smaller than that of uncracked concrete, the interpretation of

bending moment along the pile would depend on the magnitudes of the bending rigidity of concrete at different stages.

As the soil slip was not anticipated in the pile design, only nominal 0.5% steel reinforcement (ultimate tensile strength 410 N/mm^2) was provided in the piles. For a 900-mm diameter bored pile, its ultimate bending moment capacity, M_{ult}, is determined to be about 520 kNm. On the other hand, the cracking moment, M_{cr}, of the pile can be calculated by Eq. (1) according to Kong and Evans (1987)

$$M_{cr} = f_{ct}Z \quad (1)$$

where

f_{ct} = tensile strength of concrete in flexure or the modulus of rupture of concrete and equal to $0.623f'^{0.5}_{c}$ (MPa)

f'_c = characteristic strength of concrete Grade 35 (MPa),

Z = section modulus ($=I_g/y$)

I_g = gross moment of inertia

y = distance from the centroid of the section to the extreme fiber in tension

For the 900-mm diameter bored piles, its cracking moment is determined to be 264 kNm, which is about half of the pile ultimate moment value. Initial cracks would develop along the pile once the cracking moment is reached.

Moment of inertia

Gross or uncracked moment of inertia, I_g

A pile nominally reinforced with 0.5% steel can be considered as a lightly reinforced pile. Branson (1977) established that for lightly reinforced concrete structures, the gross moment of inertia, I_g of the section can be used without considering the contribution of the steel reinforcement. The I_g for a circular section is given by

$$I_g = \frac{\pi d^4}{64} \quad (2)$$

Fully cracked moment of inertia, I_{cr}

As there is already a reliable equation developed by Kong and Evans (1987) to calculate the cracked moment of inertia, I_{cr}, of a rectangular beam section, it is thus assumed that the fully cracked moment of inertia, I_{cr} for the circular bored pile can be similarly represented based on the principle of conservation of cross-sectional area. For a fully cracked section, the stresses in the steel and concrete are assumed to be proportional to strain. The cracked moment of inertia, I_{cr}, of a rectangular section is given by Kong and Evans (1987) as follows

$$I_{cr} = bd^3\left[\frac{1}{3}\left(\frac{x}{d}\right)^3 + \alpha_e\rho\left(1-\frac{x}{d}\right)^2 + \alpha_e\rho'\left(\frac{x}{d}-\frac{d'}{d}\right)^2\right] \quad (3)$$

where

$\alpha_e = \frac{E_s}{E_c}$ (modular ratio)

$\rho = \frac{A_s}{bd}$ (ratio of compression steel)

$\rho' = \frac{A_s'}{bd}$ (ratio of tension steel)

d = effective depth

d' = depth from compression zone to centroid of compression steel

x = depth of neutral axis

b = width of concrete section

According to Eqs. (2) and (3), the I_g and I_{cr} of the 900-mm bored pile are 0.03221 m^4 and 0.00607 m^4, respectively.

Effective moment of inertia, I_e

Bending moment is induced on a pile when subject to lateral soil movement. If the bending moment exceeds the cracking moment, M_{cr}, of the pile, cracks would start to develop. Nevertheless, the depth and width of cracks may vary, depending on the final bending moment distribution along the pile. As such, the moment of inertia for this partially cracked section is somewhat between I_g and I_{cr} values. Therefore, an effective moment of inertia, I_e, should be employed in the analysis of a partially cracked section. By adopting an empirical equation proposed by Branson (1977), Reese (1997) provided values of effective moment of inertia, I_e, that would reduce gradually with increasing bending moment as follows

$$I_e = \left[\frac{M_{cr}}{M}\right]^3 I_g + \left[1 - \left(\frac{M_{cr}}{M}\right)^3\right] I_{cr} \leq I_g \quad (4)$$

where M_{cr} and M are the cracking moment and applied moment, respectively.

Curvature of pile shaft

In the present study, the strain gages were fastened at the opposite faces of the reinforcement cage and perpendicular to the excavation. As strain is a function of the stress and the Young's modulus of steel, E_s, the curvature, ψ, of the pile can be obtained from the sum (if different signs) or difference (if similar signs) in the measured tensile strains, ε_t, and compressive strain, ε_c, of the steel reinforcement divided by the distance between them (Poh et al. 1999)

$$\psi = \frac{\varepsilon_t - \varepsilon_c}{d - d'} \quad (5)$$

The 75-mm diameter in-pile inclinometer tube was fastened to the bored pile reinforcement cage so that both the in-pile inclinometer tube and the pile would deflect in unison when subject to lateral displacement. This would then provide a

near-continuous set of data of pile curvature so as to deduce a more accurate and consistent bending moment profile.

In general, inclinometer readings are more reliable in determining the back-analyzed bending moments as compared to strain gage readings, as the inclinometer readings obtained along a pile are near-continuous. Poh et al. (1999) established that high order polynomials are necessary to fit the measured pile deflection profiles. In the present study, a 7^{th} order polynomial function is found to be sufficient to obtain a good fit between the measured and fitted deflection profiles. Subsequently, differentiating the pile deflection profile twice would give the curvature along the pile.

Procedure to determine pile bending moment

With the curvature and the bending stiffness of the pile determined, the bending moment, M, can be calculated based on Macaulay's method (Kong and Evans, 1987) as follows

$$M = \psi E_c I_e \quad (6)$$

In computing the bending stiffness, the value of Young's modulus E_c is assumed to remain constant (Reese, 1997). The E_c for concrete used is taken as 32 GPa.

As both M and I_e are mutually dependent [Eqs. (4) and (6)], an iterative process is performed to obtain the two parameters. Starting from I_g, this value is then substituted in Eq. (6) (where I_e=I_g). The M value obtained is then substituted in Eq. (4). The I_e value obtained is substituted back in Eq. (6). These iterative steps are repeated until both M and I_e register no further changes in values. This process is repeated for all other elevations until the entire bending moment profile is determined.

Fig. 9 shows several computed profiles of I_e values along the length of the instrumented rear pile when subject to increasing lateral soil movements for various construction activities outlined in Fig. 5. Fig. 9 reveals some important observations:

a) On Day 0, when the 3.5 m deep excavated slope failed in front of the instrumented pile group, considerable increase in pile lateral deflections was observed all the way down to about 13 m depth. This depth corresponds to the soft marine clay (N<4) and loose clayey sand (N<10) strata. The lateral soil movements diminished beneath 13 m depth when medium dense to dense sand (30<N<50) was encountered.

b) The rate of decrease of I_e values with respect to depth was the largest up to about 6 m depth which coincided with the final excavation depth in front of the instrumented pile. Within this depth, the development of cracks in the pile increased with increasing excavation depth owing to increasing lateral soft clay movements.

c) Consistent patterns of concave (curved inwards) I_e profiles are observed between depths of about 10 m and 17 m that correspond to the distinct change in soil layers from loose clayey sand (N=5) to dense sand (N=38). This aspect will be further addressed in the subsequent analysis of pile bending moment.

d) Further to the above observations, the rear pile seems to experience negative deflection (kick-back) within the dense and very dense sand strata. The pile kick-back has an average magnitude of 2.6 mm with a maximum value of 3.8 mm. It would seem that cracks along the pile in this region may have just been initiated, presumably due to the mobilization of passive resistances to resist the increasing lateral soil movements experienced by the upper portion of the pile.

Equivalent effective moment of inertia, $I_{e(equiv)}$

As cracks gradually develop along the pile due to increase in excavation depth and thus increase in lateral soil movement, the moment of inertia of the pile is expected to deteriorate further. An "equivalent" or representative average $I_{e(equiv)}$ value on a particular day can be determined using the average I_e values obtained between Day 0 of soil slip and the day of interest. Table 1 reveals that the magnitudes of the calculated $I_{e(equiv)}$ values based on the iterative calculation process described earlier, decrease over time due to increasing lateral soil movement imposed on the pile. Such a method has also been successfully used by Reese (1997) to analyze the crack behavior of laterally loaded piles. In many practical situations, the zone of maximum bending moment may occupy only a small fraction of the pile length. Reese (1997) reported that the errors due to the use of constant equivalent EI in the majority of regions of lower bending moment were deemed to be small. As such, the average $I_{e(equiv)}$ method shall be used in subsequent sections to back-analyze the effect of lateral soil movement on the pile using a well-established numerical method.

Minimum deflection and bending moment initiating pile cracks

As stated earlier, the cracking moment for the 900-mm diameter bored piles is determined to be 264 kNm. By differentiating the appropriate measured pile deflection profile twice, the corresponding pile bending moment profile that initiates cracking can thus be back-analyzed as shown in Fig. 10. It is observed that the maximum positive pile bending moment occurs at 13.5 m depth which coincides with the distinct soil interface between depths of 10 m and 13.5 m as described earlier. At this soil interface, it is expected that the pile curvature changes abruptly due to a distinct increase in soil stiffness, thus inducing the maximum pile bending moment.

Typically, pile heads are tied to the pile cap with relatively high percentage of steel. Therefore, despite experiencing bigger negative bending moment at the pile cap

level as evidenced in Fig. 10, this is often not as critical as the maximum positive bending moment developed along the lower pile shaft with only nominal steel reinforcement.

Observation of different degrees of cracking along pile length

Different degrees of cracking along the length of the pile can be demonstrated in Fig. 11, whereby the ratio of the back-analyzed bending moment, M and the cracking moment, M_{cr} is plotted against the ratio of the measured deflection, D and the initial deflection at the onset of cracking, D_i at various elevations for the back-analyzed pile responses between Day 0 and Day 37.

It is evident that three distinct zones can be identified from Fig. 11. Zone 1 can be identified as the zone whereby the pile experiences minimal cracking. This coincides with data points measured at 15 m depth with dense clayey sand layer having N value between 29 and 50. The higher resistance offered by the sand and the attenuated lateral soil movements prevents the pile from being deflected excessively.

The measured data points in Zone 2 are obtained from the pile responses at depths of 3 m, 5 m and 9 m. It is evident that these data points are somewhat nestled between the two extremes of Zones 1 and 3. These depths are dominated by the soft marine clay with little soil resistance as compared to that of the sand in Zone 1. It is deduced that cracking of the pile material is on-going for this zone.

Zone 3 represents the measured data points obtained from the pile responses at depth of 12.5 m, which approximately coincides with the soil interface as described earlier where maximum pile bending moment develops. As such the M/M_{cr} and D/D_i ratios are the greatest in Zone 3 as compared to those in Zones 1 and 2.

The pile behavior at different degrees of cracking shown in Fig. 11 shows similar trends as those reported by Branson (1977). This bilinear moment-deflection

curve suggests that the pile moment capacity reduces with increasing load levels and the pile deflection increases in tandem with increasing degree of cracking of the pile material. This would transform the relevant segment of the pile from an initial uncracked pile (Zone 1) with minimal cracking to that of an intermediately cracked pile segment (Zone 2) and finally to a fully cracked pile segment (Zone 3) whereby significant cracking has taken place.

Based on the understanding above, the cracked pile can be physically represented in a schematic plot as shown in Fig. 12(a) after having experienced lateral soil movements for 37 days. In this case, the concrete between cracks may still be capable of carrying some tension. As a result, the actual effective moment of inertia, I_e, will be somewhat in between the uncracked, I_g, and the fully cracked, I_{cr} values. Branson (1977) mentioned that in such a situation, the moment of inertia used to represent the entire pile would be the average effective moment of inertia, I_e. The significance of using an average I_e value for the entire pile length is to ensure a smooth bending moment profile. Such a method has also been used by Reese (1997) to analyse the cracking behaviour of laterally loaded piles. The method used by Reese (1997) employed the average observed deflection, the applied loading and iteration to find the values of the average EI and the corresponding values of maximum bending moment that fitted the results. Therefore, the average $I_{e(equiv)}$ values that have been determined in Table 1 will now be used in the numerical back-analysis. The concept of transforming the various moment inertia values of a pile due to varying crack intensities to its idealized, single equivalent $I_{e(equiv)}$ value for back-analysis purpose, is further illustrated in Fig. 12(b).

Numerical analysis

The numerical method developed by Chow and Yong (1996) as described in detail in Ong et al. (2006) is used to back-analyze the measured field results. The pile is modeled as a series of linear elastic beam and the soil is idealized using the modulus of subgrade reaction. The numerical analysis requires the knowledge of the pile flexural rigidity, E_pI_p, the limiting soil pressures, p_y that acts on the pile, the distribution of lateral soil stiffness, K_h with depth and the lateral soil movement profile at the pile location. The rigidity of the pile cap is determined to be $2.7x10^7$ kNm^2. The modulus of elasticity for concrete, E_c, used is 32,040 MPa, while the moment of inertia values with respect to elapsed number of days can be found in Table 1.

In most practical situations, the post-excavation vane shear strength profiles are usually not available. Leung et al. (2006) reported that the normalized limiting soil stress coefficient P_n for piles subject to lateral soil movement along the pile shaft is lower and as given in Eq. (7) (unlike piles subject to lateral load at or above the ground level).

$$P_n = p_y/c_u = 6 \quad (7)$$

where

p_y = limiting soil stress

c_u = pre-excavation vane shear strength.

The problem in hand is very similar to the centrifuge model study reported by Leung et al. (2006) as both cases involve large-strain soil movement due to excavation failure in soft clay. The Singapore marine clay is modeled as having pre-excavation vane shear strength, c_u, of $0.25\sigma'_{vo}$, where σ'_{vo} is the effective overburden stress.

The distribution of lateral soil stiffness with depth, K_h, is assumed to be related to the Young's modulus of the soil, E_s, (Chow and Yong 1996), as shown in Eq. (8).

$$K_h \cong E_s \quad (8)$$

For lateral loading, E_s of clay is assumed to range from 150 c_u to 400 c_u (Poulos and Davis 1980). In the present back analysis, E_s is taken as 300 c_u. Subsequent analyses reveal that the numerical calculation is not sensitive to the magnitude of E_s/c_u as the problem in hand involves large-strain soil movement. Instead, the more sensitive parameter would be the P_n ratio adopted in Eq. (7).

The input green field soil movement profiles are obtained from the in-soil inclinometer readings shown in Fig. 7(b). However, based on the study of Ong et al. (2009) and Lim (2001), a soil moderation factor should be considered for the rear piles. Since the soil movement occurred first at the location nearer to the excavation face, the front piles tend to shield the rear piles from the increasing soil movements due to excavation. The progressive soil movements acting first on the front pile and later on the rear pile have been captured schematically in Fig. 5. In the back-analysis of centrifuge test results under similar soil and pile configuration, Ong et al. (2009) established that a soil moderation factor of 0.7 should be applied to the soil movement profile for the rear pile.

The evaluation of limiting soil stress, p_y and the concept of average equivalent effective moment of inertia, $I_{e(equiv)}$ described above, shall now be validated using the numerical method mentioned earlier.

Calculated pile responses

Figs. 13 and 14 show a comparison of measured and predicted pile bending moment and deflection profiles due to lateral soil movement from Day -1 to Day 14,

and from Day 16 to Day 36, respectively. In general, it can be observed that the shapes of the profiles and the locations of their maxima are in good agreement. It is noted that the numerical prediction generally under-estimates the maximum negative bending moment values at the pile cap level. The measured maximum negative bending moments are much higher due to the stiffening effect caused by the provision of greater steel reinforcement to connect the pile head to the pile cap during construction. However, this stiffening effect could not be exactly modeled in the numerical back-analysis.

Since there is no in-pile inclinometer in the front pile, only discrete bending moment values measured by the strain gages are plotted for comparison in Figs. 13 and 14. The measured average strain gage readings used for the bending moment interpretation are shown in Table 2. The measured bending moment values show reasonably good agreement with the bending moment profiles predicted using the numerical method.

Figs. 13 and 14 also show the measured deflection profiles of the rear pile, which was instrumented with an in-pile inclinometer. It is observed that the shapes of the measured and predicted rear pile deflection profiles are generally in good agreement. Nonetheless, it has also been found that the rear pile deflection profiles have been slightly under-predicted between Day -1 and Day 14 (see Fig. 13), but slightly over-estimated between Day 16 and Day 36 (see Fig. 14). It is established that the accuracy of the calculated pile deflection profiles depends on the soil moderation factor used in the numerical back-analysis. Therefore, it is to be acknowledged that the value of 0.7 currently adopted seems to be a suitable average value to produce comparable predicted pile deflection profiles for all the calculated I_e values in this study.

For the sake of completeness, the calculated front pile deflection profiles are also included in Figs. 13 and 14. However, no comparison could be made because the front pile was not instrumented with an in-pile inclinometer.

Before Day 15

For relatively small lateral soil movements, Ong et al. (2006) reported that the calculated pile responses depend more on the values of bending stiffness E_cI adopted. Since the calculated and measured pile bending moments and deflections are generally comparable as illustrated in Fig. 13, the credibility of the computed average $I_{e(equiv)}$ values proposed in Table 1 (assuming E_c to be constant) used for the numerical back-analysis is therefore justified.

From Day 16 onwards

It was evident from Fig. 8 that from Day 15 onwards, the 9 m thick soft clay had moved ahead of the pile. This relative movement was more pronounced especially for the first 6 m soft clay stratum, which also coincided with the 5 m excavation depth. This important observation points to the onset of the soil flow phenomenon, where the soil stresses are expected to have reached their limiting values. Such phenomenon had been observed and documented by Leung et al. (2006), thus justifying the use of P_n value of 6 in the numerical analysis, whereby reasonably good agreement between calculated and measured pile responses had been demonstrated (see Fig. 14).

Therefore from Day 15 onwards, it is strongly believed that the pile has fully cracked at the Zone 3 segment as a result of increasingly larger lateral soil movements. This observation is also supported by the fact that when I_{cr} is used in the numerical analysis from Day 15 onwards, reasonably good comparison between calculated and measured pile responses can be observed, as demonstrated in Fig. 14.

Fig. 14 also evidently shows that the ultimate rear pile bending moment (520 kNm) is exceeded between Day 23 and Day 30. This postulation signifies that the instrumented pile group was damaged by the excessive soil movement caused by the failure of the clay slope. Therefore, the pile group is deemed unfit to carry the designed column load and a replacement pile group is indeed necessary. In this case study, the mobilization of pile axial load as a result of the soil movement could not be practically measured from the current instrumentation program. Also, the numerical method did not consider the possible development of additional axial load due to the soil movement. Through observation, the soil movement occurred more significantly in the lateral direction than the vertical direction. As such, it is expected that the increase in the pile axial load will not be significant.

In summary, Fig. 15 shows the deterioration of the pile moment of inertia from an initially uncracked pile to a partially cracked pile and finally to a totally cracked pile due to increasing lateral soil movement as the excavation depth increased. When localized excavation was carried out between Day 8 and Day 14 to expose some pile heads at the toe of the slope, the deterioration of the instrumented pile moment of inertia was minimal. Subsequently, when further slope excavation was carried out between Day 15 and Day 18, it was observed that the deterioration of pile moment of inertia continued, but at a much faster rate. Finally, I_{cr} was reached after 16 days of excavation since the soil slip. From Fig. 15, it is obvious that the pile moment of inertia varies due to cracking as a result of the progressive soil movements experienced by the clay slope. If the variations in pile moment of inertia are not considered in the analysis, the pile bending moment will be over-predicted and the pile deflection will be under-predicted since the pile is assumed to be stiffer than what

it is (Ong et al., 2010). This will result in an unrealistic and over-conservative back-analysis.

Conclusions

The pre- and post-failure behaviors of a full-scale instrumented cast in-situ concrete 4-pile group subject to excessive lateral soil movement triggered by a slope failure are investigated in detail in this paper. The pile undergoes transformation from initially an uncracked pile to one that is partially cracked and finally to a fully cracked pile, due to large-strain lateral soil movement acting on the pile group over the excavation period. With the progressive development of cracks along the pile, the present study details a procedure in determining suitable average equivalent effective moment of inertia, $I_{e(equiv)}$ values for use in the back-analysis of the field data.

It is established that the computed $I_{e(equiv)}$ values and the normalized limiting ratio of soil stress to vane shear strength, P_n, ratio of 6 as recommended by Leung et al. (2006), are suitable to be employed in the numerical method adopting the green field lateral soil movements to predict the behavior of the pile group subject to increasing lateral soil movements. With reasonably good agreement between the measured and predicted pile bending moment as well as deflection profiles, it thus reflects the validity of combining the concepts of $I_{e(equiv)}$ and P_n. The consistency of the measured pile behavior in the field with the results of the centrifuge tests conducted by Ong et al. (2006, 2009) and Leung et al. (2006) has further reinforced the understanding of the concept of soil limiting stress and the corresponding behavior of piles subject to lateral soil movements.

References

Branson, D. E. (1977). *Deformation of concrete structures.* New York: McGraw-Hill.

Chow, Y. K. and Yong, K. Y. (1996). "Analysis of piles subject to lateral soil movements." *J. Inst. of Eng. Singapore*, 36 (2), pp. 43-49.

Kong, F. K. and Evans, R. H. (1987). *Reinforced and prestressed concrete.* 3rd Edition. Van Nostrand Reinhold (U.K.) Co. Ltd.

Leung, C. F., Ong, D. E. L., and Chow, Y. K. (2006). "Pile behavior due to excavation-induced soil movement in clay. II: Collapsed wall." *J. Geotech. Geoenviron. Eng.*, 132(1), pp. 45-53.

Lim, J. K. (2001). "Behaviour of piles subject to excavation-induced soil movement." M.Eng Thesis, National University of Singapore.

Ong, D. E. L., Leung, C. F. and Chow, Y. K. (2006). "Pile behavior due to excavation-induced soil movement in clay. I: Stable wall." *J. Geotech. Geoenviron. Eng.*, 132(1), pp. 36-44.

Ong, D. E. L., Leung, C. F. and Chow, Y. K. (2009). "Behavior of Pile Groups Subject to Excavation-Induced Soil Movement in Very Soft Clay". *J. Geotech. Geoenviron. Eng.*, 135(10), pp. 1462-1474.

Ong, D. E. L., Leung, C. F. and Chow, Y. K. (2010). "Effect of limiting soil pressure on pile group adjacent to a failed excavation". Proc. of Int. Conf. on Geotechnical Challenges in Megacities, Moscow, Russia, Vol. 3, pp. 785-792.

Ong, D. E. L., Leung, C. F. and Chow, Y. K. (2011). “Behavior of Pile Groups Subject to Excavation-Induced Soil Movement in Very Soft Clay”. Discussion by F. Castelli & Closure, *J. Geotech. Geoenviron. Eng.,* 137(1), pp. 110-113.

Poh, T. Y., Goh, A. T. C., Wong K. S., Wong, I. H. and Poh, K. B. (1999). “Determination of BM in diaphragm wall.” Field Measurements in Geomechanics, Singapore, pp. 229-234.

Poulos, H. G., and Davis, E. H. (1980). *Pile foundation analysis and design*. John Wiley & Sons, New York.

Reese, L. C. (1997). "Analysis of laterally loaded piles in weak rock”. *J. Geotech. Geoenviron. Eng.,* 33(11), pp. 1010-1017.

Table 1

Table 1. Computed average equivalent effective moment of inertia, $I_{e(equiv)}$ and fully cracked moment of inertia, I_{cr}

No. of days after first soil slip	**Computed moment of inertia, I (m^4)**
Day -1	$I_{e(equiv)}$ = 0.01921
Day 1	$I_{e(equiv)}$ = 0.01486
Day 9	$I_{e(equiv)}$ = 0.01003
Day 14	$I_{e(equiv)}$ = 0.01000
Day 16	I_{cr}= 0.00616
Day 18	
Day 19	
Day 23	
Day 30	

Table 2

Table 2. Measured average strain gage readings used for bending moment interpretation

	Average Strain, ε							
	Depth of strain gage in instrumented Rear Pile				Depth of strain gage in instrumented Front Pile			
	6m	8m	9m	11m	6m	8m	9m	11m
Day -1	2.55E-05	2.15E-05	-2.08E-04	3.17E-04	-4.50E-06	-1.10E-05	-1.39E-04	2.35E-05
Day 1	1.90E-05	2.95E-05	-3.02E-04	-7.55E-05	-1.60E-05	1.22E-04	-1.12E-04	6.40E-05
Day 9	-2.66E-04	2.98E-04	4.09E-04	6.69E-04	-1.33E-03	6.40E-05	-8.05E-05	1.05E-04
Day 14	-6.69E-04	2.11E-04	4.11E-04	5.18E-04	-1.48E-03	-4.71E-04	-1.03E-04	1.14E-04
Day 16	-6.66E-04	2.22E-04	2.84E-04	8.10E-04	-1.52E-03	-7.00E-04	-8.85E-05	1.24E-04
Day 18	-6.74E-04	1.93E-04	3.97E-04	9.93E-04	-1.64E-03	-1.11E-03	-3.55E-05	9.45E-05
Day 23	-9.51E-04	2.50E-06	4.03E-04	1.19E-03	-1.71E-03	-1.70E-03	-1.25E-05	-4.25E-04
Day 30	-9.84E-04	-8.30E-04	4.11E-04	1.02E-03	-2.01E-03	-2.19E-03	5.60E-05	-1.01E-03
Day 36	-1.11E-03	-2.67E-03	3.29E-04	1.02E-03	-3.08E-03	-2.17E-03	-4.94E-04	-1.03E-03

Figure 1

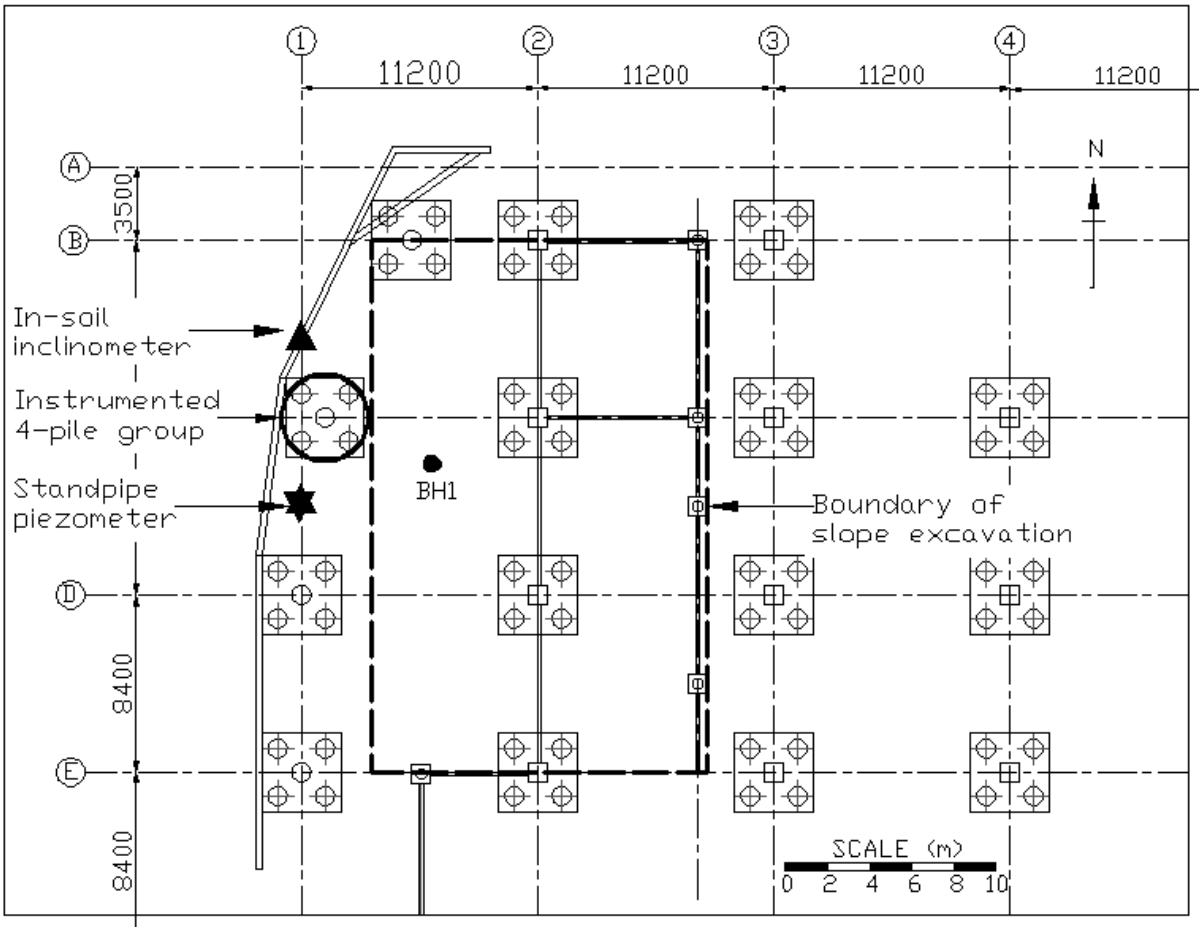

Fig. 1. Plan view showing the locations of instruments and instrumented pile group at the site

Figure 2

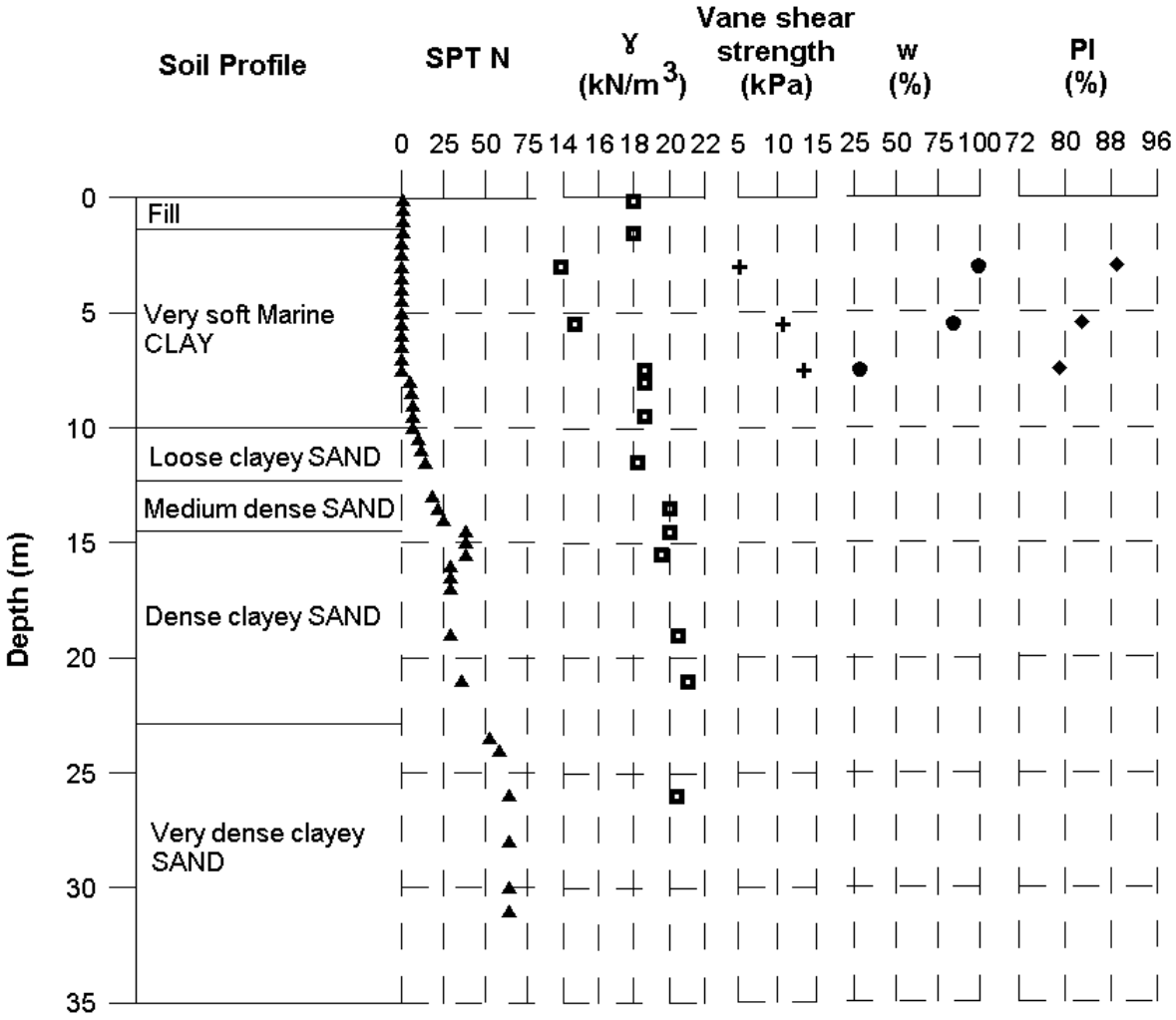

Fig. 2. Interpreted subsurface soil profile at site

Figure 3

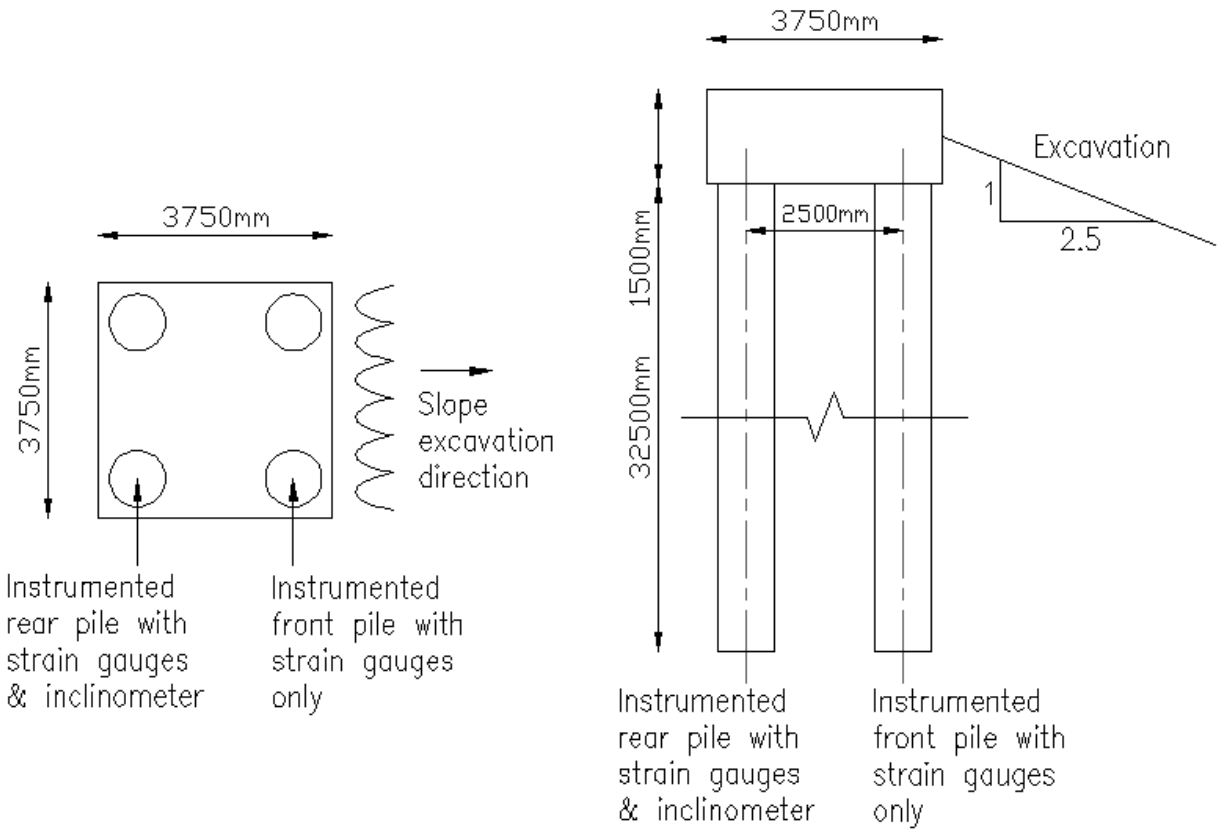

Fig. 3. Plan and elevation views of instrumented pile group with respect to the slope excavation

Figure 4

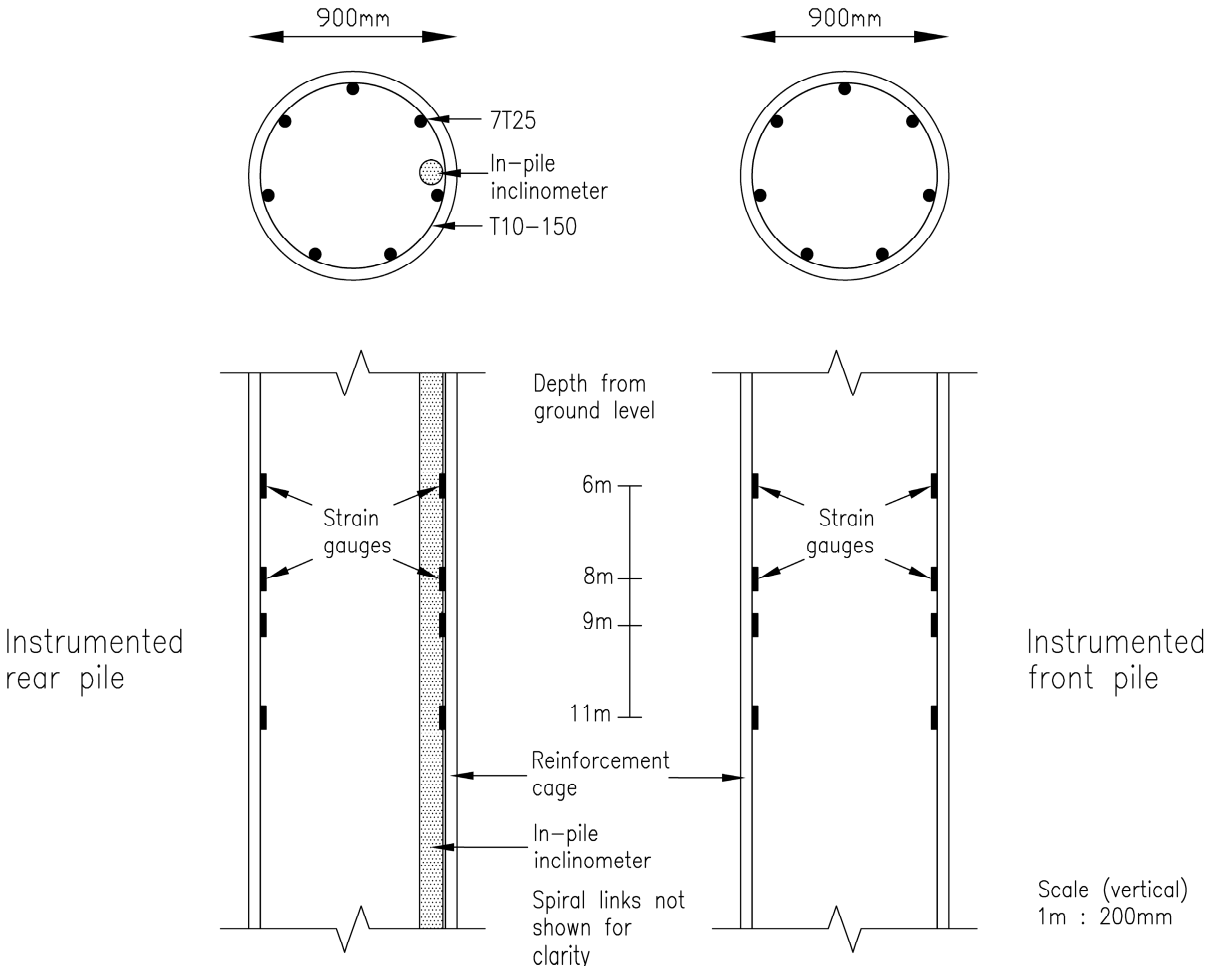

Fig. 4. Layout of instruments attached to reinforcement cages of the bored piles

Figure 5

Stage	Day	Key Event	Construction Sequence
1	Day 0	Soil slip occurred	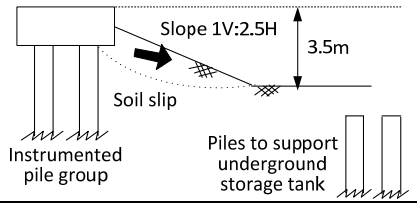
2	Days 1-7	Soil movement due to excavation of slope, sheet pile installed	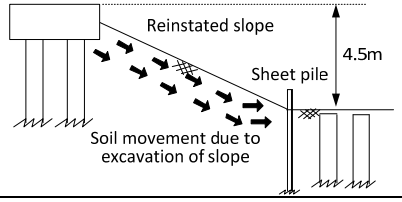
3	Days 8-14	Localized excavation to expose installed pile heads	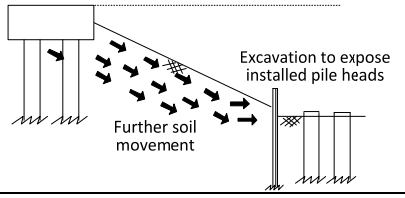
4	Days 15-18	Further excavation to 5.0m depth	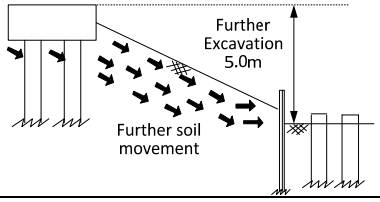
5	Days 19-21	Further excavation to 5.5m depth & temporary struts installed	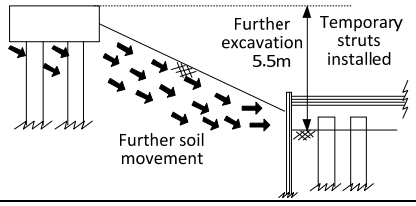
6	Days 22-29	Further excavation to 6.0m depth	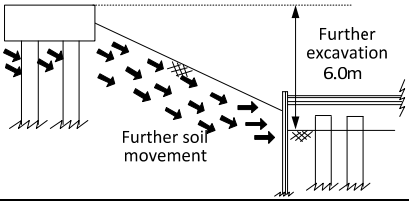
7	Days 30-62	Casting of pile caps & further works	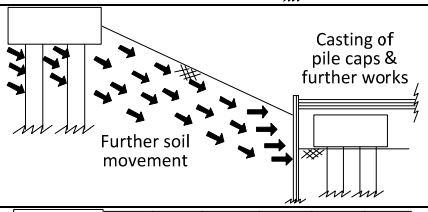
8	Day 63	Backfilling works	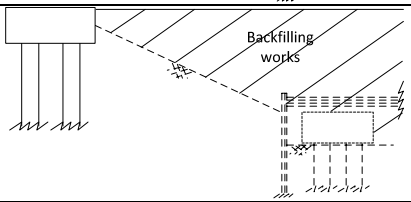

Fig. 5. Timeline of excavation works

Figure 6

Fig. 6. Slope failure that unexpectedly occurred next to the instrumented pile group (Day 0)

Figure 7

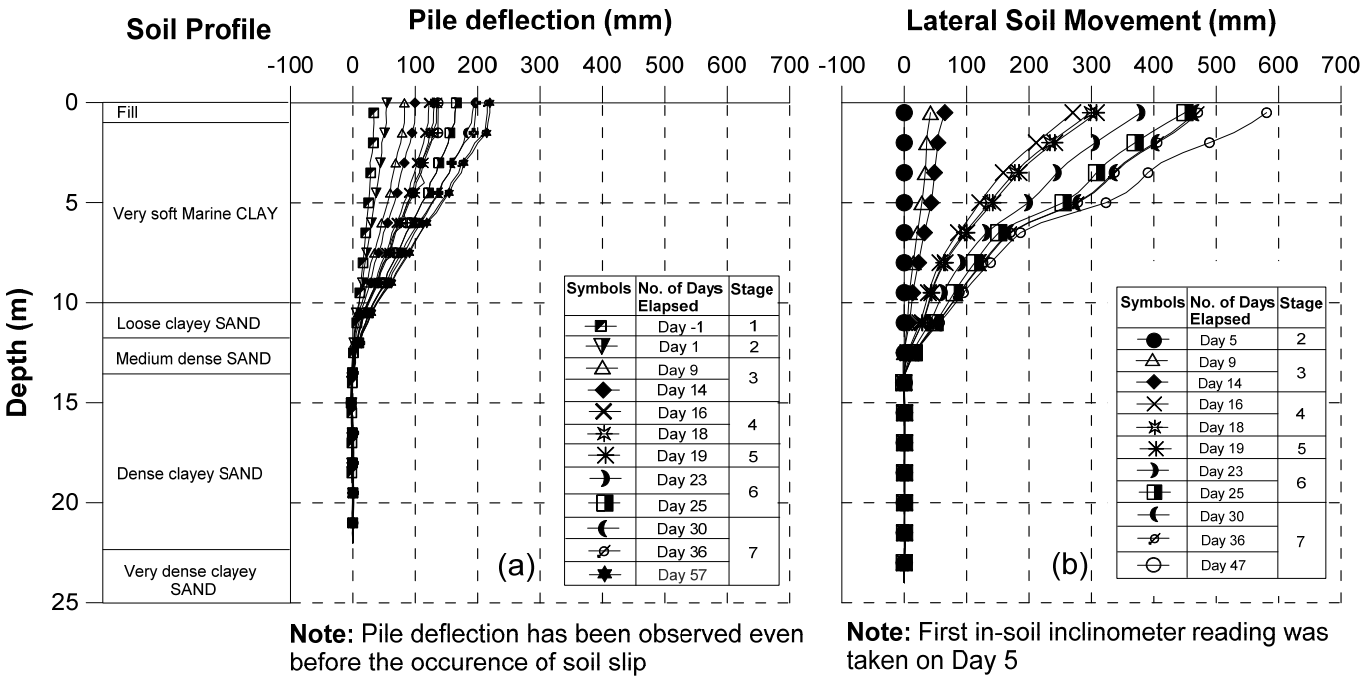

Fig. 7. Measured (a) rear pile deflection and (b) lateral soil movement profiles over the excavation period

Figure 8

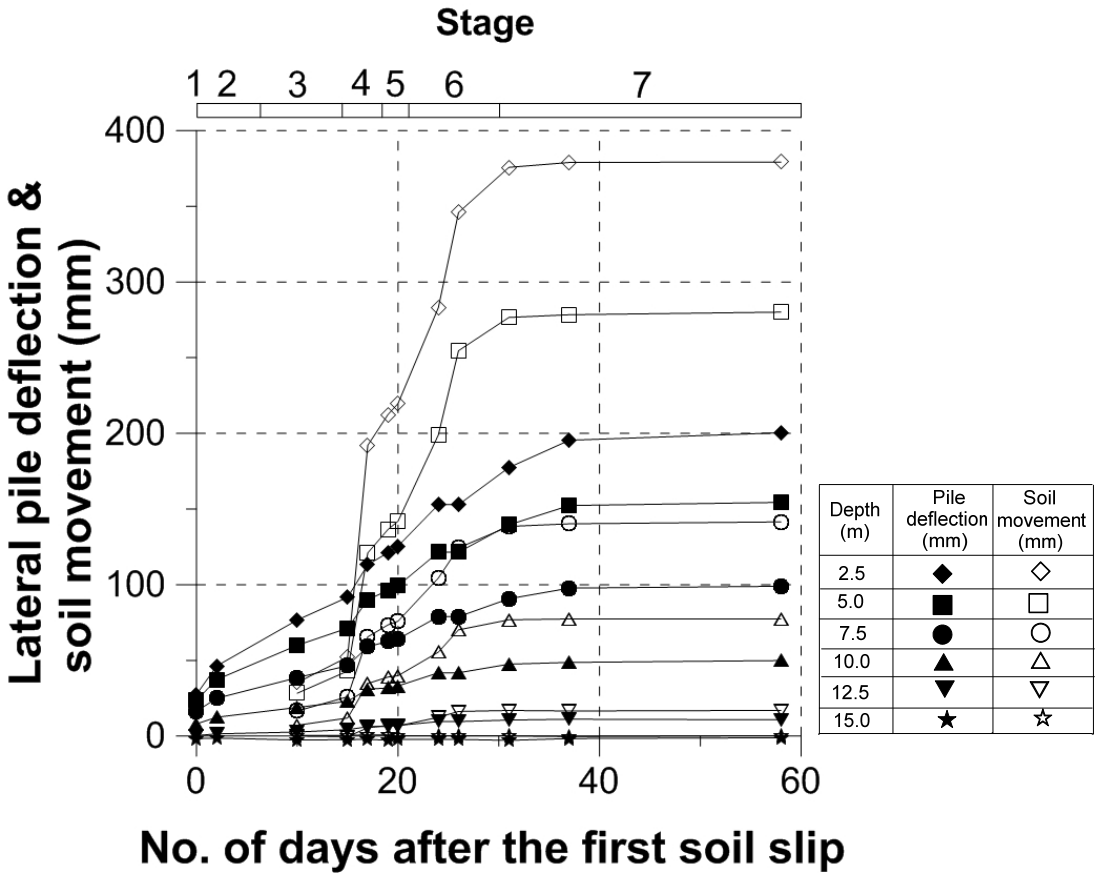

Fig. 8. Measured lateral pile deflection and soil movements at various depths over the excavation period

Figure 9

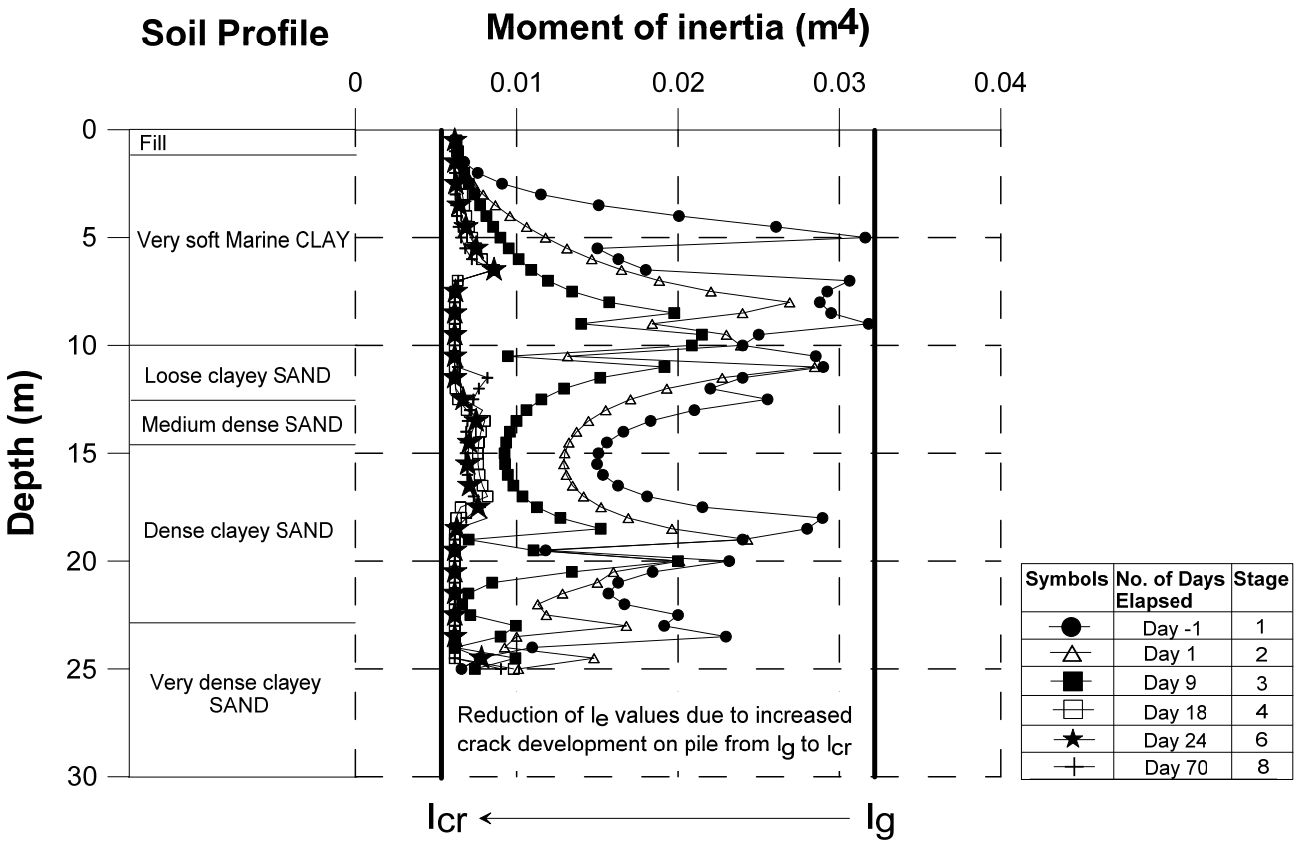

Fig. 9. Computed profiles of effective moment of inertia, I_e along the instrumented rear pile over the excavation

Figure 10

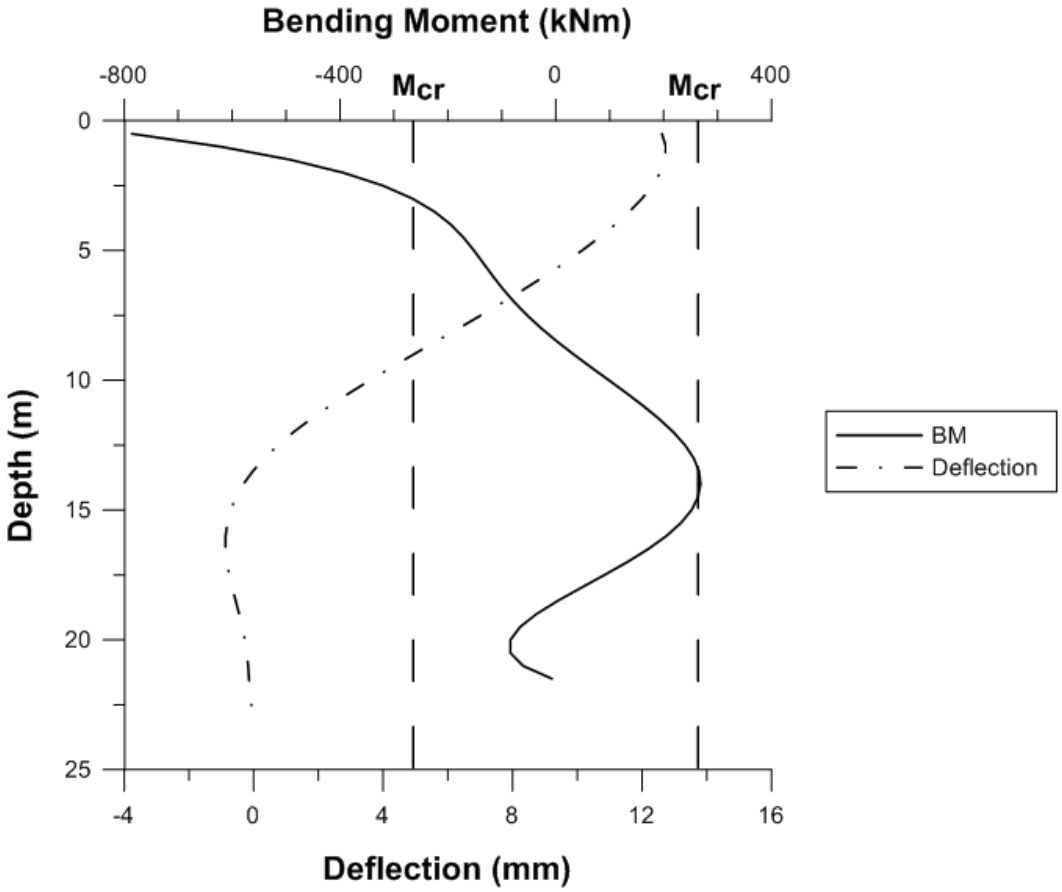

Fig. 10. Back-analyzed pile deflection and bending moment profiles that initiate cracking

Figure 11

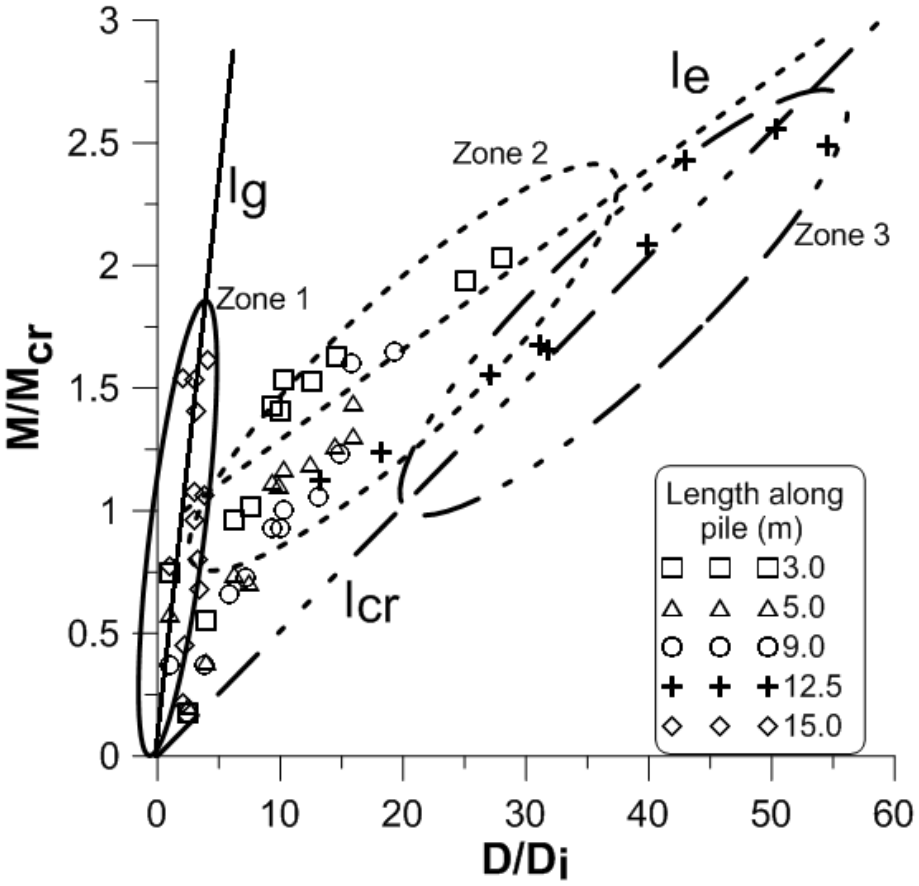

Fig. 11. Interpreted bi-linear moment-deflection curve

Figure 12

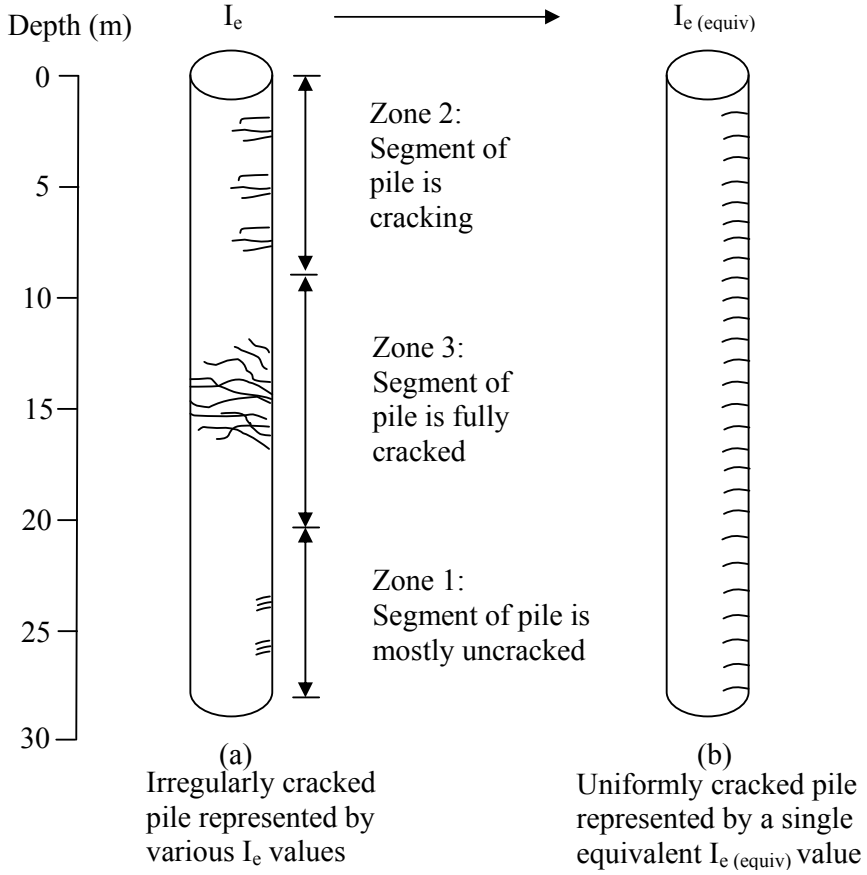

Fig. 12. (a) Possible development of different crack intensities on the instrumented pile and (b) an idealized cracked pile used for back-analysis

Figure 13

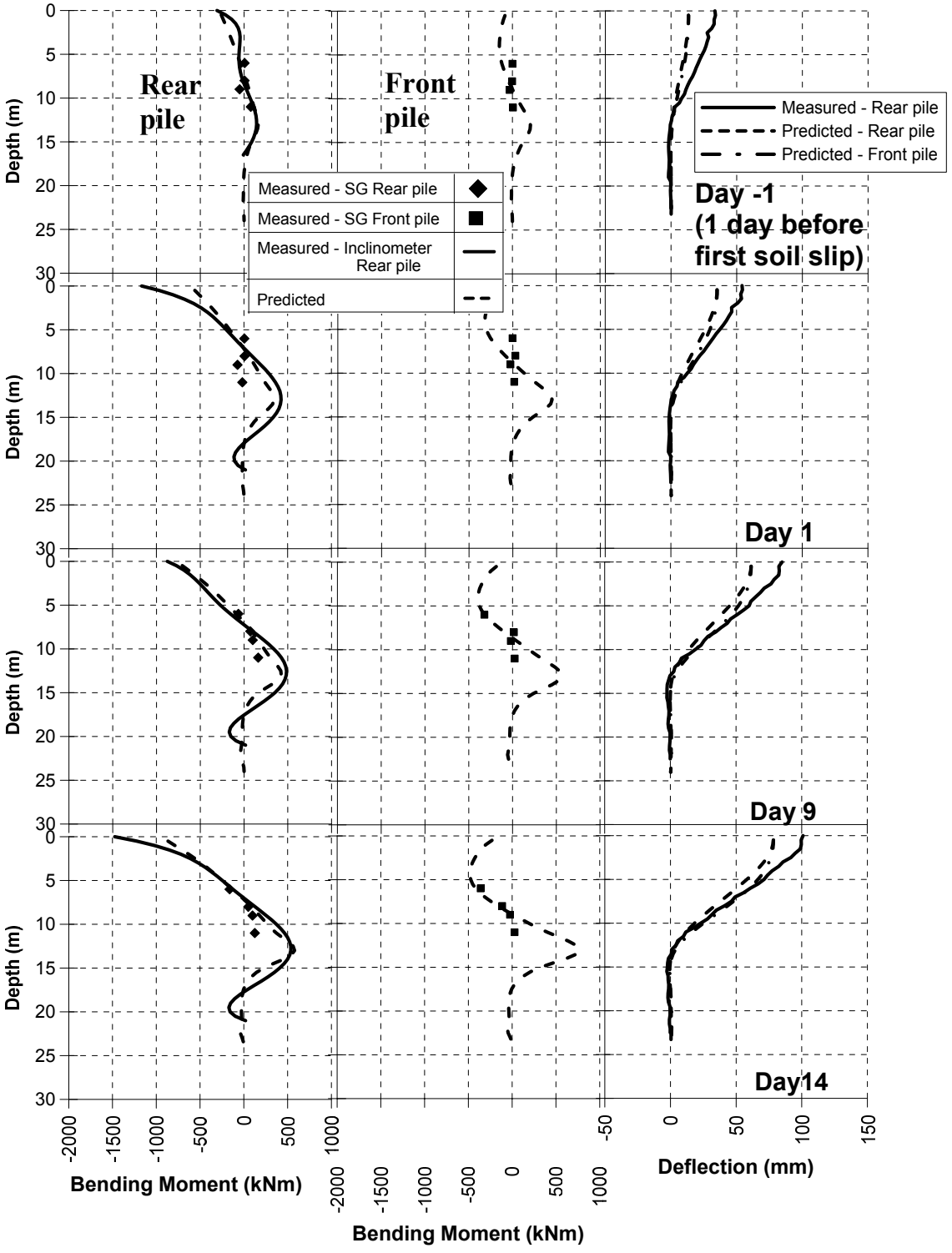

Fig. 13. Selected measured and predicted pile bending moment and deflection profiles based on computed average $I_{e(equiv)}$ before and on Day 14

Figure 14

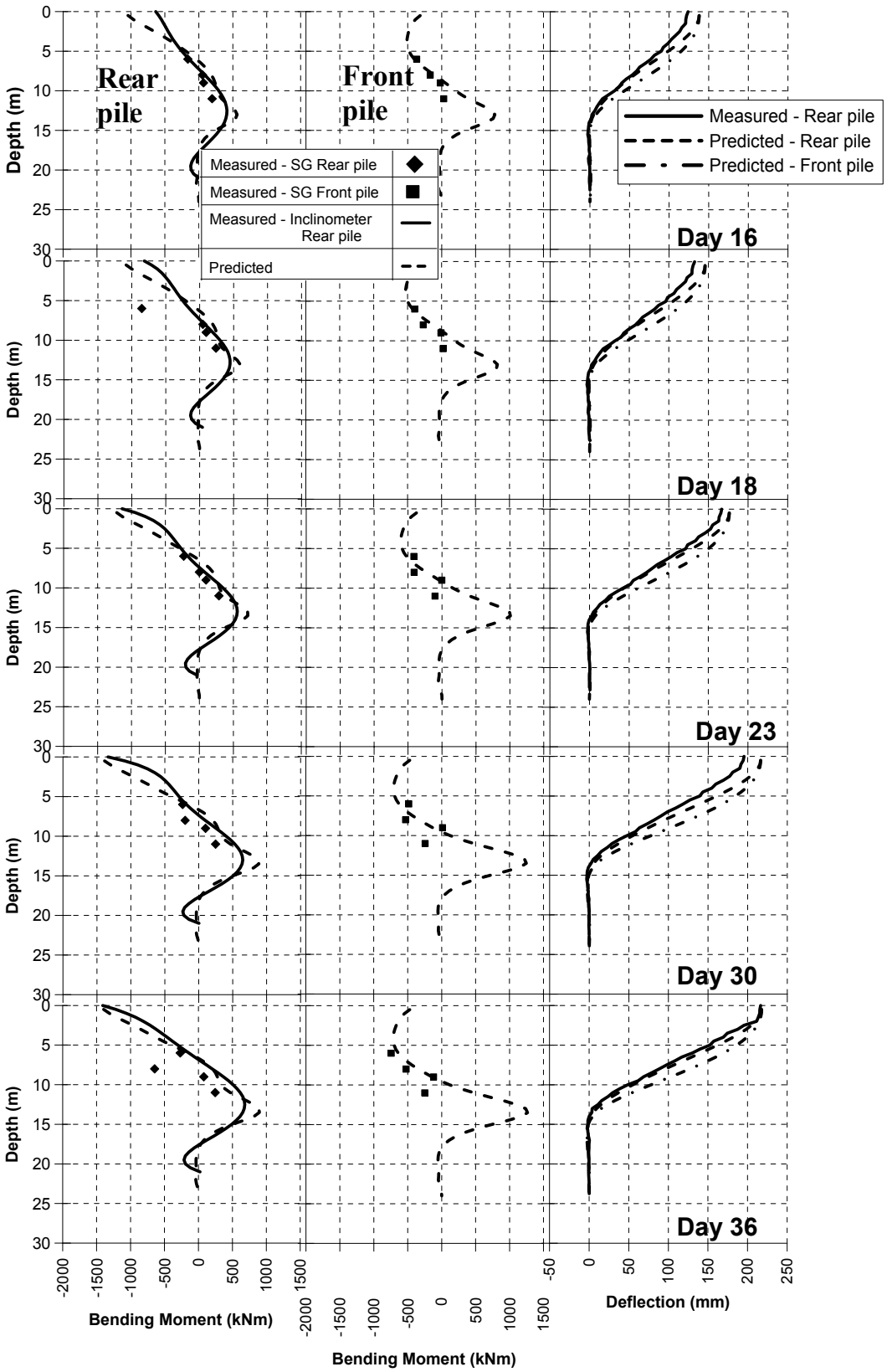

Fig. 14. Selected measured and predicted pile bending moment and deflection profiles based on I_{cr} after Day 15

Figure 15

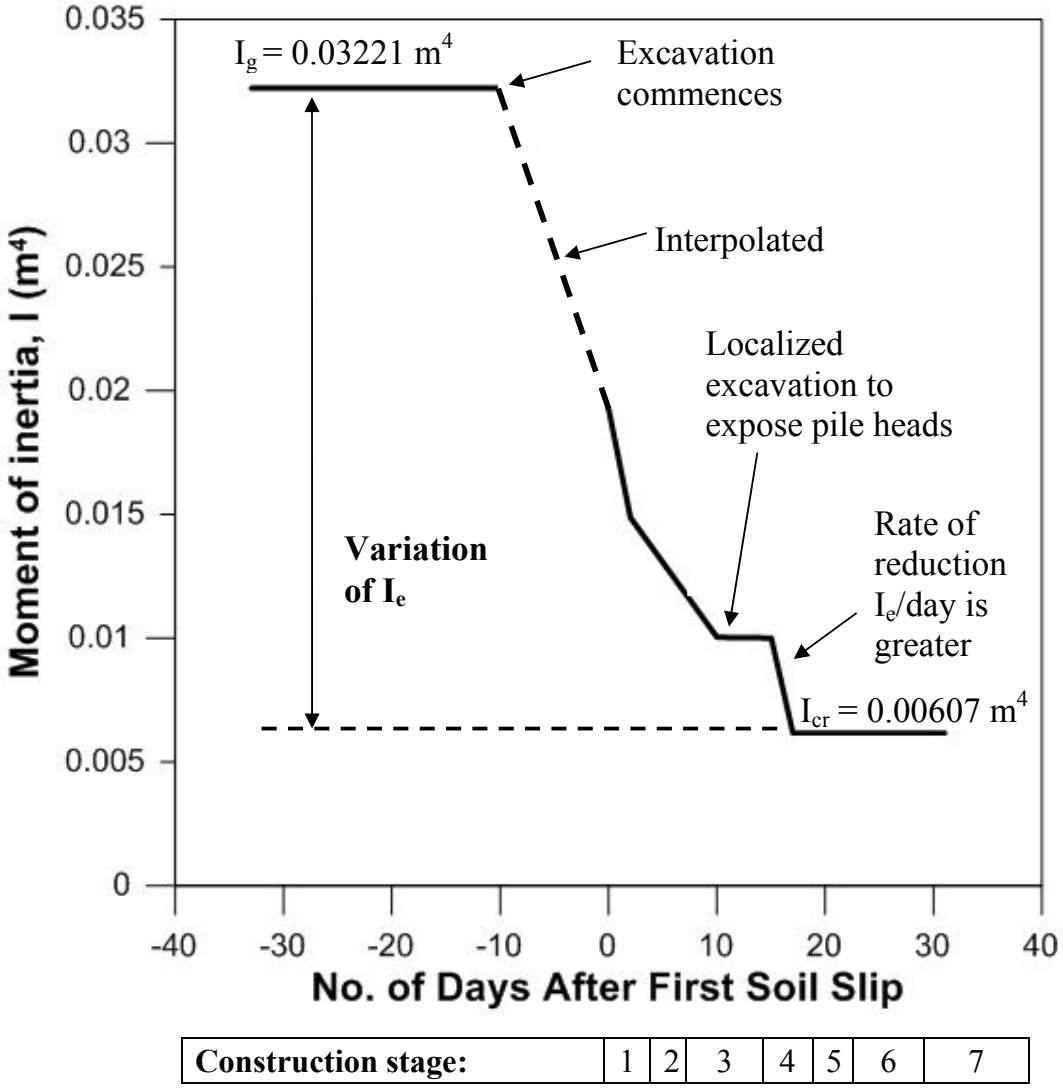

Fig. 15. Deterioration of pile moment of inertia after soil slip

List of Figures

Fig. 1. Plan view showing the locations of instruments and instrumented pile group at the site

Fig. 2. Interpreted subsurface soil profile at site

Fig. 3. Plan and elevation views of instrumented pile group with respect to the slope excavation

Fig. 4. Layout of instruments attached to reinforcement cages of the bored piles

Fig. 5. Timeline of excavation works

Fig. 6. Slope failure that unexpectedly occurred next to the instrumented pile group (Day 0)

Fig. 7. Measured (a) rear pile deflection and (b) lateral soil movement profiles over the excavation period

Fig. 8. Measured lateral pile deflection and soil movements at various depths over the excavation period

Fig. 9. Computed profiles of effective moment of inertia, I_e along the instrumented rear pile over the excavation period

Fig. 10. Back-analyzed pile deflection and bending moment profiles that initiate cracking

Fig. 11. Interpreted bi-linear moment-deflection curve

Fig. 12. (a) Possible development of different crack intensities on the instrumented pile and (b) an idealized cracked pile used for back-analysis

Fig. 13. Selected measured and predicted pile bending moment and deflection profiles based on computed average $I_{e(equiv)}$ before and on Day 14

Fig. 14. Selected measured and predicted pile bending moment and deflection profiles based on I_{cr} after Day 15

Fig. 15. Deterioration of pile moment of inertia after soil slip

List of Tables

Table 1. Computed average equivalent effective moment of inertia, $I_{e(equiv)}$ and fully cracked moment of inertia, I_{cr}

Table 2. Measured average strain gage readings used for bending moment interpretation